J Therm Anal Calorim (2010) 101:1155–1160
DOI 10.1007/s10973-010-0805-x

Development of a model for compensating the influence of temperature gradients within the sample on DSC-results on phase change materials

Greg Albright · Mohammed Farid · Said Al-Hallaj

Received: 5 January 2009 / Accepted: 13 April 2010 / Published online: 5 May 2010

Abstract The use of phase change materials (PCMs) in thermal storage is not a new concept, but engineers are continually finding new ways to utilize them in a wide range of applications. A PCM takes advantage of high latent heat in the phase change process to store large amounts of heat while undergoing only a small change in temperature. This property makes PCMs suitable for thermal storage purposes in a wide range of engineering applications. Due to the nature of these applications, it is vital to have a precise knowledge of the thermal characteristics of any PCM. Unfortunately, due to the low thermal conductivities and high latent heats found in PCMs, current measuring tools such as differential scanning calorimetry, provide inconsistent results. This paper conjectures that these errors come from the effects of low thermal diffusivity samples as well as improper data analysis methods.

Keywords DSC · Differential scanning calorimetry · PCM · Phase change material · Gradient · Latent heat

Introduction

The term "Phase Change Material" is applicable to any material; however, in this case, it refers to materials that are able to absorb large amounts of heat during the phase change process. The phase change process in this context is most commonly melting/solidification. The ability to store large amounts of heat in a small temperature range is advantageous for applications where heat is produced and temperature stability is desired. One example is PCM impregnated wallboard. PCM impregnated wallboard can store and release heat at the desired room temperature, keeping the temperature stable and reducing heating and cooling costs [1]. Commonly used PCMs are paraffins, salt hydrates, and fatty acids [2]. This work focuses on paraffin PCMs due to their widespread availability and absence of major supercooling phenomena which can be found in salt hydrates [3]. Future works may attempt to address salt hydrates.

In order to maximize the benefit of PCMs, it is necessary to know their precise melting/freezing temperature range, latent heat, and specific heat. Currently, these values are measured using a variety of thermal instruments, the most popular being differential scanning calorimetry (DSC). This paper focuses more specifically on the heat flux type DSC. As the name implies, DSC is a differential method that compares the temperature responses of two materials to a programmed heat treatment. The basic layout of the DSC can be described as a small cylindrical oven with the heat being provided from the furnace wall through a known heat resistance to the sample and reference. The key components of the interior can be seen in Fig. 1. Cut out from the constantan plate are two circular platforms approximately 6 mm in diameter. The sample, which is usually about 5 mm in diameter and 0.5 mm thick, is encased in a circular aluminum pan and placed on top of one platform. The sample mass can vary from 1 to 40 mg. An empty aluminum pan is placed on the other platform and serves as the reference. Thermocouples are located under the center of each platform.

The most common heat program is to increase the heating plate temperature at a constant rate. The properties

G. Albright · M. Farid (✉)
Department of Chemical & Materials Engineering, School of Engineering, The University of Auckland, Private Bag 92019, Auckland, New Zealand
e-mail: m.farid@auckland.ac.nz

S. Al-Hallaj
AllCell Technologies LLC, 2321 W. 41st Street, Chicago, IL 60616, USA

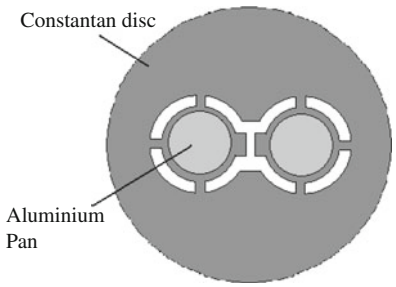

Fig. 1 DSC interior

of the reference material are known, thus the difference between responses of the reference and the sample can be used to determine the sample's properties. The DSC process works well for materials of high thermal diffusivity, however, test results are inconsistent for PCMs due to their low thermal conductivities and high latent heats. The results have shown that the calculated effective specific heat capacity and melting range of a PCM, based on the DSC temperature data, are very sensitive to heating rate and sample mass; however, the sensitivity of the latent heat is still debatable. The effective specific heat capacity is different than the sensible specific heat capacity because it includes the phase change effects. Integrating the area between the effective specific heat capacity and baseline specific heat capacity in the melting range results in the latent heat. Figure 2 shows the results from a DSC test done on a PCM according to tests done by ZAE Bayern reported in a white paper entitled "Determination of the Heat Storage Capacity of PCM and PCM-Objects as a Function of Temperature". Ideally, the curves would be identical for different heating rates and sample masses.

It seems that an easy solution to the problem is to just use low heating rates; however, as the heating rate decreases, the signal becomes noisier and the tests take longer to conduct. Furthermore, the high heating rate data can be useful for application in real world situations, such as lithium ion battery cooling, where the PCM is subjected to high heating rates. The effective specific heat capacity can be viewed as a function of heating rate and temperature as opposed to just temperature. This concept is supported by Castellon et al. [4] in an analysis of using a heat flux DSC to determine the enthalpy of paraffin wax.

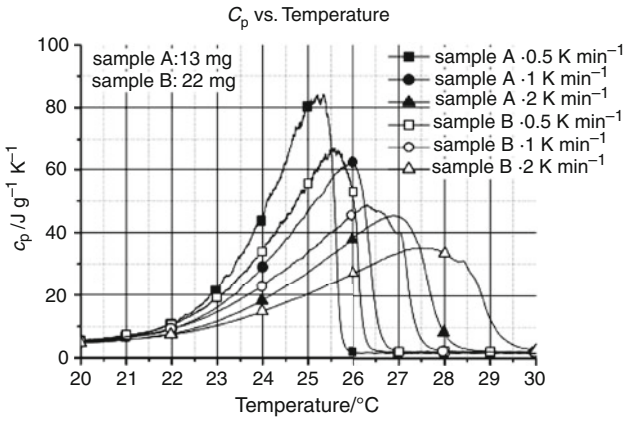

Fig. 2 Results for the heat capacity of a PCM determined using a DSC in dynamic mode with varying heating rates and sample mass

This problem has been discussed by Greco and Maffezzoli [5]. They argue that the effective specific heat capacity and melting temperature range are functions of the heating rate, but that the DSC machine measures the correct latent heat at any heating rate. Other authors have come to similar conclusions that samples with high thermal diffusivity will cause inaccurate melting range and specific heat measurements in the DSC process, but do little to address the latent heat issue [6–8]. Some of the errors in DSC can be corrected through modifications to the hardware, but it does not appear that there are any modifications that can completely account for the temperature gradient [10]. Abdulkarim and Ghazali [11] found experimentally that fast scan rates do lead to depressed latent heat values. Elsaesser et al. [12] found that high heating rates can lead to thermal lag, but for their experimental sample, the lag was negligible at a 10 K/min scan rate.

Method

In order to properly understand what is happening within a DSC sample, it is necessary to build a model that replicates the current process. The model used for this work focuses on the heating cycle of the DSC process, but the results are applicable for the cooling process as long as the material does not experience supercooling. From the heat flux type DSC geometry, it is known that the sample radius is much larger than the thickness. Due to this condition, any heat flux in the radial direction will be insignificant when compared to heat flux in the axial direction, thus a 1D axial cylindrical conduction model is a suitable base.

$$\frac{\partial T}{\partial t} = \alpha \frac{\partial^2 T}{\partial z^2} \tag{1}$$

Due to the fact that the aluminum pan contacts the cylindrically shaped sample at the top and the bottom ends of the sample and the thermal diffusivity of aluminum is 4 orders of magnitude higher than that of the PCM, it can be assumed that the entire aluminum pan is at a constant temperature. This condition means that the heat flux at the top and bottom of the sample will be identical and symmetry can be utilized to simplify the computation. This assumption is agreed upon by Greco and Maffezzoli [5]. The model sample is cut in half and a heat flux is applied at

one end while an adiabatic boundary is applied at the other, which was formerly the center of the sample.

$$-k\frac{\partial T}{\partial z} = q'' \quad \text{at} \quad z = 0 \tag{2}$$

Where $z = 0$ is the interface between the heating plate and the sample.

$$\frac{\partial T}{\partial z} = 0 \quad \text{at} \quad z = \frac{L}{2} \tag{3}$$

Where L is the thickness of the sample.

The sample and reference are supplied with specific heat capacity, thermal conductivity, and density values. A desired temperature rise rate is input and the heat flux is calculated based on temperature differences between the sample, reference, and heating plate. From the geometry previously described, the following schematic represents the heat flow (Fig. 3).

The general equation for the heat flux between two bodies at temperatures T_A and T_B is:

$$q''_{AB} = \frac{T_A - T_B}{R} \tag{4}$$

where R is the thermal resistance between the two points. For the DSC setup, this equation becomes:

$$q''_S = q''_R + \frac{T_R - T_S}{R} \tag{5}$$

where q''_R is the heat flux entering the reference sample, T_R and T_S are the surface temperatures of the reference and the sample, respectively. No specific data was found regarding the thermal resistance between the platform and base plate, so the value was approximated based on DSC geometry and materials. Using the lumped capacitance method, the resistance is estimated to be 105 K/W. Eqs. 1–4 were discretized using one dimensional implicit finite difference method and solved in matrix form.

At this point, the model can calculate the heat input and temperature at any location in the sample. From this information, the simulated effective specific heat capacity of the sample, c_S, can be calculated as a function of temperature.

$$c_S = \frac{q_S \Delta t}{m \Delta T_S} \tag{6}$$

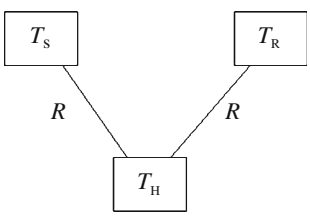

Fig. 3 Thermal circuit

The deviation of this simulated effective c_S from the effective c_p that was input by the user as a material property is affected by heating rate and mass. The effective c_p input by the user is a sixth order polynomial over the temperature range from 50 to 63.3 °C, starting at 6.05 J/gK and ending at 5 J/gK with a peak of 32.16 J/gK. The polynomial c_p curve, which closely resembles the 0.5 K/min curve in Fig. 5, is an effective way to simulate the latent heat of melting. Integrating the c_p curve gives the heat absorbed during melting of the PCM. Figure 4 is an example heat flow versus time curve from the Shimadzu DSC manual. The baseline heat flow curve, AC, represents what the heat flow value would be if there was no melting. The integrated area between curves AC and ABDC provides information for calculating the latent heat. How line AC is determined is vital to the results and is seldom straightforward when real DSC data for PCM is analyzed. The difference in the definition of this line is the source of the difference between the results produced in this work versus those previously published.

Also important from Fig. 4 is the melting range, which starts at point P. This point is established by drawing a line tangent to where the c_p plot reaches a constant slope, point B, and determining where the line intersects segment AC, points P. As can be seen, this process is not very precise and leaves much open to the visual interpretation of the user; however, the main source of error in the melting range measurement is due to the thermal gradients within the sample that will be discussed shortly.

Results

The model was used to determine the changes in the measured effective c_p curve and measured latent heat values as a function of sample size and heating rate. Figure 5 shows the results of simulations for a 24 mg sample at heating rates varying from 0.5 to 10 K/min.

It is clearly seen that the simulated effective specific heat capacity of the sample and the melting range are very sensitive to the heating rate; a problem which is exacerbated as the sample size increases. Table 1 shows the

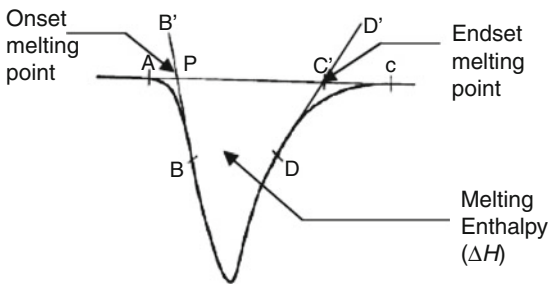

Fig. 4 DSC melting curve

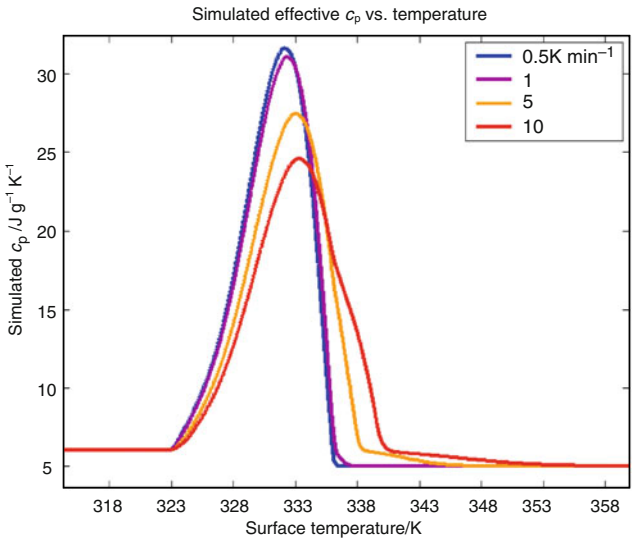

Fig. 5 c_p versus temperature (24 mg)

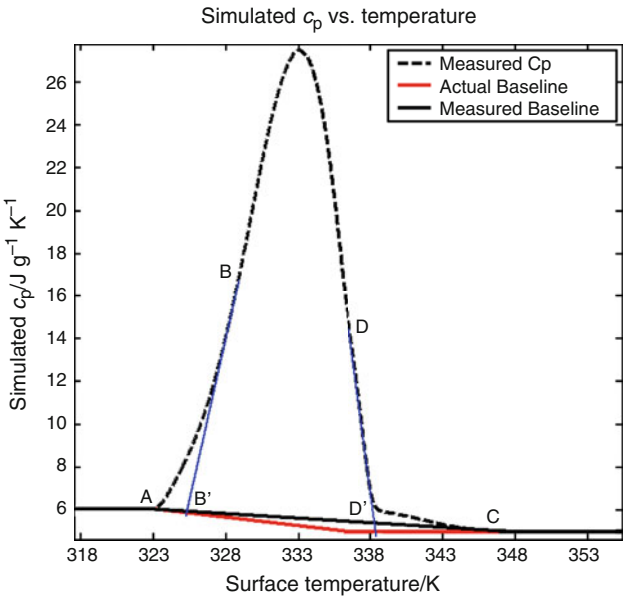

Fig. 6 Effect of baseline

Table 1 Melting temperature range

Rate/K min^{-1}	T_{onset}/°C	T_{endset}/°C
0.5	50	63.2
1	50	63.5
5	50	65
10	50	67.2

Table 2 Latent heat as function of baseline

Heating rate/K min^{-1}	Method 1	Method 2
0.5	173.7	173.8
1	173.1	173.8
5	168.6	174.2
10	164.1	174.6

melting range data derived from Fig. 5 by the methods previously described. The ideal melting range for the PCM polynomial curve used in the model is 50–63.1 °C.

As stated before, the latent heat is the integration of the c_p versus temperature graph. The results are subject to where the DSC user defines the limits of the range, but more importantly, how the baseline AC is determined [9]. In Fig. 6, the two baseline options are drawn. The black baseline is the one that the user creates in the experimental DSC process by connecting points A and C. The red line is the actual baseline of the material, which for the model was determined from the input effective c_p curve for the PCM modeled. The DSC technician would have no way of knowing the latter baseline. However, previous simulation work done on the DSC process has neglected the distinction between these two baselines. The researchers have used the input effective c_p baseline, rather than the DSC user defined one, causing the results to show that the measured latent heat is not a function of heating rate.

The curves from Fig. 5 were integrated over the visually determined range using the two different baseline definitions to calculate the latent heat. The results are shown in Table 2. "Method 1" is using the actual DSC baseline that the DSC user would create. "Method 2" is using the baseline that is true for the material, but unknown to the DSC user, which modelers have used. The theoretical latent heat of the simulated PCM is 174.67 J/g.

Using the DSC determined baseline, the latent heat decreases as the heating rate increases, whereas if the theoretical baseline is used, the latent heat remains fairly constant. This difference is caused by the increasing area between the two baselines as the heating rate increases.

Since the effect of sample mass is also of interest, the simulations were also run for multiple masses. Table 3 displays the latent heat values at the different heating rates and sample masses.

Figure 7 is the plot of the data from Table 3 and illustrates how latent heat is a function of heating rate and sample mass.

It can be seen from the previous data that the thermal diffusivity and heating rate do indeed influence the measured effective specific heat values, latent heat, and melting range. Further data can provide some insight into why this occurs. Figure 8 is a surface mesh plot of temperature data as a function of location in the sample and surface temperature. The temperature data is the differential temperature between the sample surface temperature and the temperature at a given z-axial location, where position 0 is the surface and position 0.5 is the center of the sample. As the sample begins

Table 3 Simulated latent heat/J g^{-1}

Heating rate/K min^{-1}	11 mg	24 mg
0.5	174.0	173.7
1	173.9	173.1
5	172.1	168.6
10	170.2	164.1

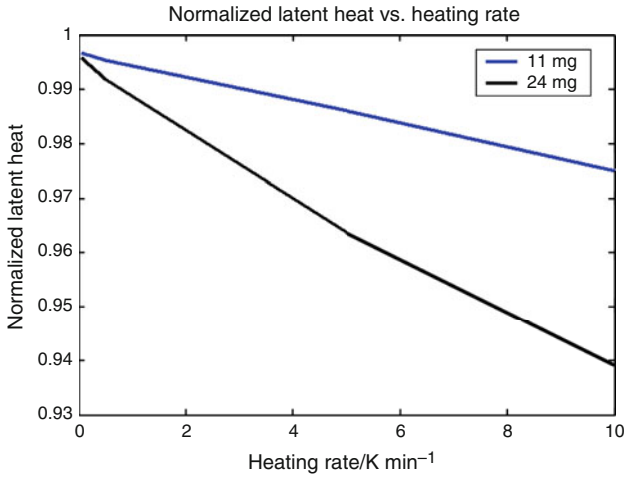

Fig. 7 Normalized latent heat vs. heating rate

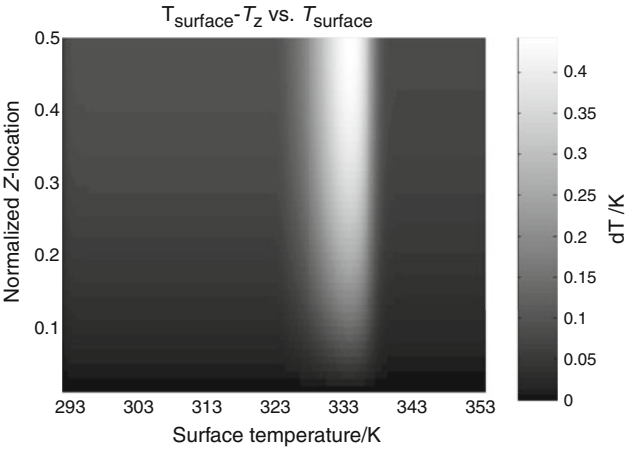

Fig. 8 $T_{surface} - T_z$

to melt, the temperature difference between the center and surface of the sample increases quickly.

Analysis

From the data collected in the simulation, it is clear that DSC provides inaccurate results for even moderate heating rates of a material with low thermal diffusivity. If the DSC process is to be used in the future, the inaccuracies must be known and accounted for.

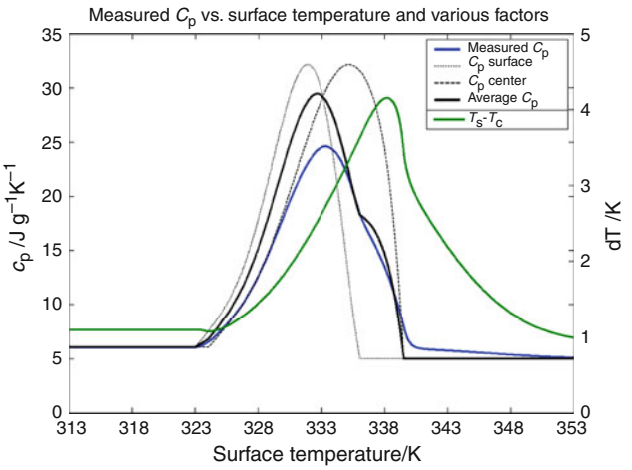

Fig. 9 Factors that influence measured c_p

Considering the factors that influence the results, it appears that the internal thermal gradient in the sample is the source of error for the effective specific heat capacity and melting range measurements. The surface heat flux causes a temperature gradient within the sample; the temperature at the center of the sample will always be somewhat lower than the surface temperature during heating. The temperature difference itself is of concern for determining the proper melting point, but the rate at which the temperature difference changes is of primary importance for c_p calculations. The DSC measures how much heat is being absorbed by the sample. To calculate the effective c_p, it assumes that this heat is uniformly heating the entire mass. Instead, during melting, the mass closest to the thermocouple is absorbing a disproportionate amount of this heat, causing the measured temperature increase produced by a certain amount of heat to be inaccurately high. An inaccurately high change in temperature reading leads to an inaccurately low measured effective c_p value. Once melting is over, the temperature gradient still exists, creating an inaccurately high measured effective c_p value until the gradient is sufficiently small. As the sample size and heating rate increase, the scale of the internal temperature gradient increases, causing even lower c_p values during melting. Figure 9 provides an illustration of these concepts. It shows the results from a trial at a higher heating rate and mass than Fig. 8, so the value of $T_s - T_c$ is higher. The "c_p surface" and "c_p center" curves show the input value of the effective specific heat capacity at those locations, which are functions of the temperature at those locations, when the surface temperature is at the value given on the lateral axis. The "average c_p" is the arithmetic average of these two curves, and represents the bulk effective c_p if there was no temperature gradient. The "$T_s - T_c$" curve is the surface temperature minus the center temperature.

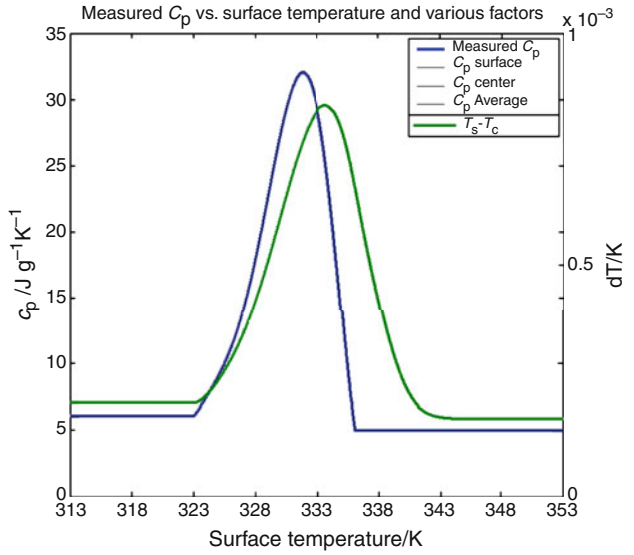

Fig. 10 Factors that influence measured c_p (high thermal conductivity)

Judging from Fig. 9, it appears that the measured effective specific heat capacity is strongly influenced by the average effective heat capacity of the bulk, but is also a function of the temperature gradient within the mass. Figure 10 is the same plot for the same test conditions as Fig. 9, but the thermal conductivity has been changed from 0.21 to 200 W/mK. Due to the high conductivity, it is impossible to see any separation between the c_p curves. The black lines and the blue line are essentially the same. The differences in the graphs illustrate the influence of the thermal conductivity on DSC results. Note that the maximum temperature difference between the surface and the center of the sample goes from 4 to 0.0008 K.

In the work reported on here, the model was constructed to use a given effective c_p curve, which is accepted to be the accurate value, to model the results of the DSC process. If the process is reversed, the model can be used to correct the DSC data. If the DSC experimental data and the sample properties (aside from effective c_p) are input, the true effective c_p curve can be calculated through a curve matching optimization process. The model will find a best fit polynomial to describe what effective specific heat curve would result in the measured DSC data under the given experimental conditions.

Conclusions

The results of the study show that the DSC process can provide inaccurate data for materials of low thermal diffusivity. The paper proposes that the errors are due to undesired thermal gradients within the sample that result in misrepresentative data. If the process it to continue to be used, these errors must be corrected. Since it is complicated to interfere with the hardware or process of DSC, the corrections must be made directly to the data afterwards. It is proposed that the data be inserted into a model that closely resembles the DSC process and the model will determine the true effective specific heat capacity and latent heat of the sample by matching the model simulation results to the actual DSC results.

Acknowledgments The authors are grateful for the financial and technical support provided by All Cell Technologies, LLC (Chicago, IL).

References

1. Farid MM. Green buildings using phase change energy storage. 3-e green building international conference, 15–18 October, 2007, Tainan, Taiwan.
2. Farid MM, Khudhair AM, Razak SA, Al-Hallaj S. A review on phase change energy storage: materials and applications. Energy Conver Manage. 2004;45:1597–615.
3. Royon L, Guiffant G. Heat transfer in paraffin oil/water emulsion involving supercooling phenomenon. Energy Conv Manage. 2001;42:2155–61.
4. Castellon C, Gunther E, Mehling H, Hiebler S, Cabeza LF. Determination of the enthalpy of PCM as a function of temperature using a heat-flux DSC—a study of different measurement procedures and their accuracy. Int J Energy Res. 2008;32:1256–65.
5. Greco A, Maffezzoli A. Correction of melting peaks of different PE grades accounting for heat transfer in DSC samples. Polym Test. 2008;27:61–74.
6. Xu SX, Li Y, Feng YP. Study of temperature profile and specific heat capacity in temperature modulated DSC with a low sample heat diffusivity. Thermochimica Acta. 2000;360:131–40.
7. Simon SL. Enthalpy recovery of poly(ether imide): experiment and model calculations incorporating thermal gradients. Macromolecules. 1997;30:4056–63.
8. Van Miltenburg JC, Cuevas-Diarte MA. The influence of sample mass, heating rate and heat transfer coefficient on the form of DSC curves. Thermochimica Acta. 1989;156:291–7.
9. Richardson MJ. Quantitative aspects of differential scanning calorimetry. Thermochimica Acta. 1997;300:15–28.
10. McMillan LC, Darvell BW. An improved cooling curve technique as applied to waxes. Meas Sci Technol. 1999;10:1319–28.
11. Abdulkarim SM, Ghazali HM. Comparison of melting behaviors of edible oils using conventional and hyper differential scanning calorimetric scan rates. ASEAN Food J. 2007;14(1):25–35.
12. Elsaesser MS, Winkel K, Mayer E, Loerting T. Reversibility and isotope effect of the calorimetric glass → liquid transition of low-density amorphous ice. Phys Chem Chem Phys. 2010;12:708–12.